Pt−Ir−IrO_2NT Thin-Wall Electrocatalysts Derived from IrO_2 Nanotubes and Their Catalytic Activities in Methanol Oxidation

Chi-Chi Shan,[†] Dah-Shyang Tsai,*[,†] Ying-Sheng Huang,[‡] Sie-Hong Jian,[†] and Chia-Liang Cheng[†]

Department of Chemical Engineering and Department of Electronic Engineering, National Taiwan University of Science and Engineering, Taipei, 106 Taiwan

Received September 2, 2006. Revised Manuscript Received November 26, 2006

The structural features and catalytic activities of PtIr electrocatalysts derived from vertical IrO_2 nanotubes (IrO_2NT) of 1100 nm in height and 80−100 nm in diameter have been studied using scanning electron microscopy, transmission electron microscopy, X-ray powder diffraction, and cyclic voltammetry toward CO_{ad} and methanol oxidation. Lattice oxygen of IrO_2NT is removed under high-vacuum thermal annealing to facilitate nucleation of 3−5 nm Ir grains and subsequent synthesis of PtIr catalyst on the tube walls. Interestingly, the apparent dimensions and orientation of IrO_2NT can be preserved via pore generation in the oxygen removal process. The tubular wall was transformed from a thin dense plate of IrO_2(110) single crystal into a porous plate consisting of connected Ir grains that exhibit lattice fringes of the Ir-{110} spacing with preferential orientation of Ir[1$\bar{1}$0] parallel to the IrO_2NT growth direction. The amount of Ir being reduced, the Ir grain size, and the deposited Pt size strongly influence the surface area and the catalytic activity. The Pt−Ir−IrO_2NT catalyst reduced at 500 °C exhibits a significantly higher activity than Pt−IrO_2NT and Pt−IrNT in methanol oxidation and also a higher current density than that of a Johnson−Matthey PtRu catalyst in the high potential region.

Introduction

The direct use of liquid alcohols as an energy carrier is a favorable option for fuel cells, in view of many difficulties associated with storage and transportation of hydrogen. Methanol receives most of the research attention because of its high-energy density and storage convenience. The success of the direct methanol fuel cell (DMFC) depends on two key materials, the membrane and the electrocatalysts. Improving the anode electrocatalyst for methanol has been one of the central issues owing to its sluggish kinetics. The unsatisfactory oxidation rate and current are mainly attributed to self-poisoning of its reaction intermediates (CO) on Pt catalyst.[1] Promotion and sustaining of the Pt activity by adding a second or a third metal appears to be an effective and long-lasting solution. Ru is found to have the largest effect.[2] The Ru promotion is intimately involved in the Pt catalyzed methanol oxidation scheme and plays a decisive role in the structural effects.[3] For instance, the initial methanol oxidation current of Pt(111) is lower than those of Pt(110) and (100), but a Ru deposited Pt(111) surface is more active than the other two.[4]

Compared with the anode catalyst of proton exchange membrane fuel cell (PEMFC), the prospect of improving the DMFC anode catalyst appears to be optimistic because the DMFC power density when using the state-of-the-art PtRu catalyst is approximately 1/10 that of the PEMFC employing the same Pt loading.[1] Recent reports suggested Ir could be a beneficial element in promoting catalytic activities of Pt and PtRu,[5] even though the earlier results indicated PtIr was significantly less active and Ir itself exhibited a low activity in methanol oxidation.[6,7] Tsaprailis and Birss prepared alloyed or partially alloyed $Pt_{1.8}Ir$ nanoparticles of size 1.5−3.5 nm using a sol−gel process.[8] They found the prepared $Pt_{1.8}Ir$ catalyst in methanol oxidation outperformed the Johnson−Matthey $Pt_{1.0}Ru_{1.0}$ catalyst (carbon dispersed) by a factor of 2.7 in the current density at 0.7 V (vs SHE). The $Pt_{1.8}Ir$ catalyst also exhibited CO tolerance so that its stability in methanol oxidation was higher than that of Pt catalyst. Sivakumar and Tricoli synthesized carbon-supported PtRuIr nanoparticles through vapor decomposition of Pt, Ru, and

* Corresponding author. E-mail address: tsai@ch.ntust.edu.tw. Phone: 886-2-2737-6618. Fax: 886-2-2737-6644.
[†] Department of Chemical Engineering.
[‡] Department of Electronic Engineering.

(1) Liu, H.; Song, C.; Zhang, L.; Zhang, J.; Wang, H.; Wilkinson, D. P. *J. Power Sources* **2006**, *155*, 95. Lamy, C.; Lima, A.; LeRhun, V.; Delime, F.; Coutanceau, C.; Leger, J. M. *J. Power Sources* **2002**, *105*, 283. Wasmus, S: Kuver, A. J. *Electroanal. Chem.* **1999**, *461*, 14.
(2) Hamnett, A. Direct Methanol Fuel Cells. In *Handbook of Fuel Cells*; Vielstich, W., Lamm, A., Gasteiger, H. A., Eds.; Wiley: New York, 2003; Chapter 18, pp 305−322.
(3) El-Shafei, A. A.; Hoyer, R.; Kibler, L. A.; Kolb, D. M. *J. Electrochem. Soc.* **2004**, *151*, F141. Gasteiger, H. A.; Markovic, N.; Ross, P. N.; Cairns, E. J. *Electrochim. Acta* **1994**, *39*, 1825. Yajima, T.; Uchida, H.; Watanabe, M. *J. Phys. Chem. B* **2004**, *108*, 2654.
(4) Herrero, E.; Franaszczuk, K.; Wieckowski, A. *J. Phys. Chem.* **1994**, *98*, 5074. Xia, X. H.; Iwasita, T.; Ge, F.; Vielstich, W. *Electrochim. Acta* **1996**, *41*, 711. Chrzanowski, W.; Wieckowski, A. *Langmuir* **1998**, *14*, 1967. Chrzanowski, W.; Kim, H.; Wieckowski, A. *Catal. Lett.* **1998**, *50*, 69.
(5) Liang, Y.; Zhang, H.; Zhong, H.; Zhu, X.; Tian, Z.; Xu, D.; Yi, B. *J. Catal.* **2006**, *238*, 468.
(6) Hamnett, A.; Kennedy, B. J. *Electrochim. Acta* **1988**, *33*, 1613.
(7) Ortiz, R.; Marquez, O. P.; Marquez, J.; Gutierrez, C. *J. Phys. Chem.* **1996**, *100*, 8389. Hefny, M. M.; Abdel-Wanees, S. *Electrochim. Acta* **1996**, *41*, 1419.
(8) Tsaprailis, H.; Birss, V. I. *Electrochem. Solid-State Lett.* **2004**, *7*, A348.

10.1021/cm062085u CCC: $37.00
Published on Web 01/13/2007

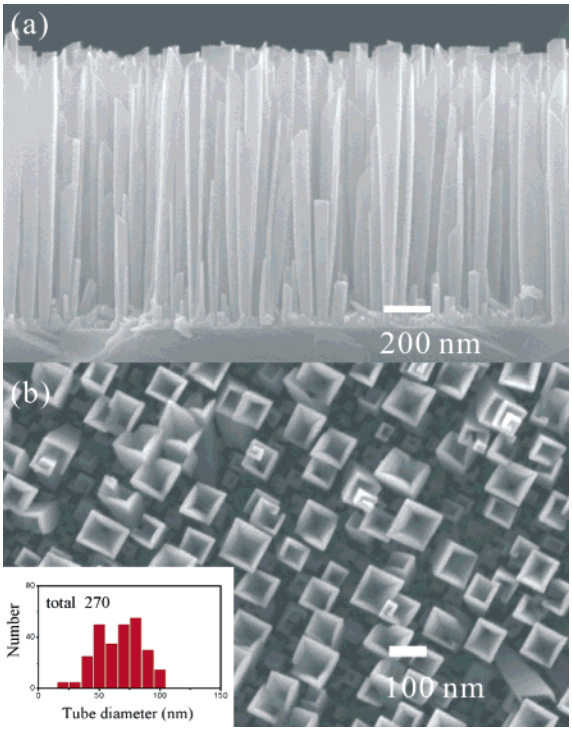

Figure 1. Morphology of Ir−IrO$_2$NT after 500 °C thermal annealing: (a) cross-sectional and (b) top views. Also shown is a histogram of the tube diameter distribution. The secondary electron image of IrO$_2$NT is virtually the same.

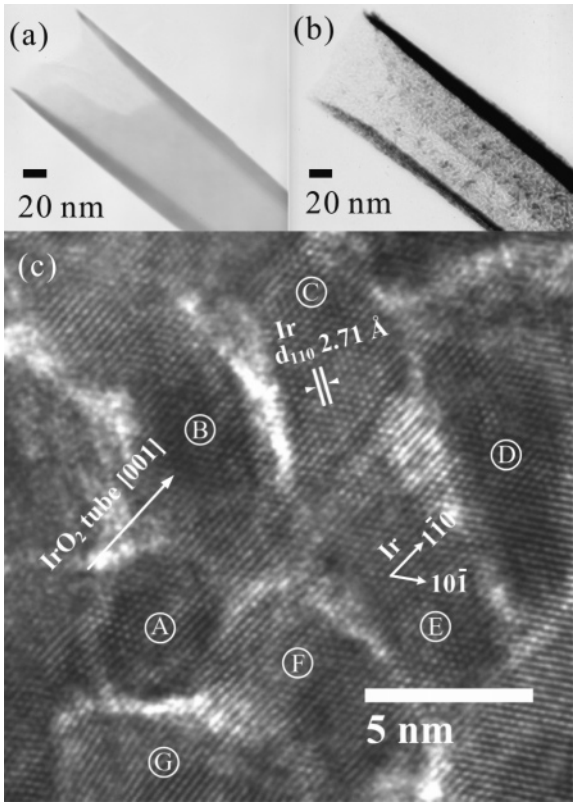

Figure 2. Structural variations in the tube wall before and after the lattice oxygen removal. Two bright-field TEM images of (a) an IrO$_2$ tube and (b) a 500 °C-reduced tube; please note the wall fragmentation in part b. The atomic image of a 500 °C-reduced tube wall in part c was taken with a zone axis of Ir[$\bar{1}$11]. Note the same lattice fringe of various Ir grains.

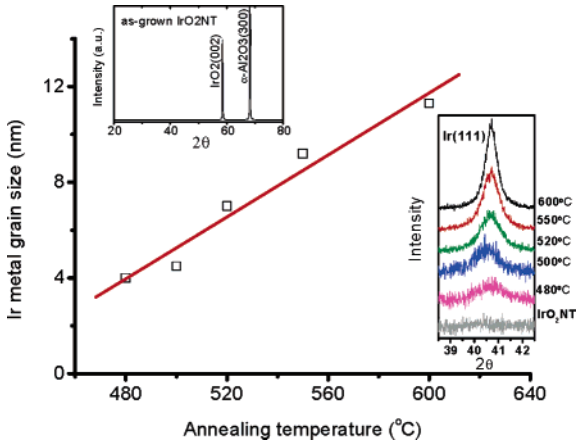

Figure 3. Ir metal crystal size increasing linearly with respect to the temperature in high-vacuum thermal annealing. The average crystal size was calculated using the Scherrer formula. Insets of the IrO$_2$NT XRD pattern and the Ir(111) reflections of various annealing temperatures are also presented.

Ir actylacetonates.[9] They found the 2.5 nm nanoparticles of Pt/Ru/Ir = 63:35:2 exhibited the catalytic activity toward methanol oxidation much higher than a commercial E-TEK catalyst. Liang et al. emphasized the Ir assistance in enhancing the CO_{ad} oxidation activity of PtRu.[5] They reported a reduction in peak potential of CO_{ad} stripping, 0.45 V (PtRu/C), 0.31 V (PtRu/C, E-TEK), and 0.25 V (PtRuIr/C) versus SCE. Chen et al. prepared a Ti−IrO$_2$−Pt electrode and found its charge-transfer resistance of methanol oxidation was reduced, compared with Pt and Ti/Pt electrodes.[10] They concluded that the IrO$_2$ presence was responsible for the homogeneous dispersion of Pt particles that led to a higher surface area and a lower potential in CO_{ad} oxidation.

In this work, we investigate the oxygen removal of IrO$_2$ nanotubes (IrO$_2$NT) and the electrochemical activity of its derived structural catalysts. IrO$_2$NT is an assembly of well-aligned square tubes which has been synthesized by reactive sputtering or metallorganic chemical vapor deposition (CVD) in the previous research.[11] Oxygen of IrO$_2$NT can be removed, and the resultant Ir grains are closely related to the crystal structure before reduction. Hence, the prepared PtIr catalysts possess a preferential surface structure. We analyze the fine structure of these catalysts and search for its connections with electrochemical properties.

Experimental Section

IrO$_2$NT was grown at 350 °C on the sapphire(100) substrate in a cold-wall CVD reactor using (methylcyclopentadienyl)(1,5-cyclooctadiene)Ir (Strem Chemicals) as the precursor. Details of growth conditions and the epitaxial relation can be found in previous publications.[11] The lattice oxygen of IrO$_2$NT was removed by annealing at a selected temperature between 400 and 600 °C in a

(9) Sivakumar, P.; Tricoli, V. *Electrochem. Solid-State Lett.* **2006**, *9*, A167.
(10) Chen, A.; LaRussa, D. J.; Miller, B. *Langmuir* **2004**, *20*, 9695.
(11) Chen, R. S.; Huang, Y. S.; Tsai, D. S.; Chattopadhyay, S.; Wu, C. T.; Lan, Z. H.; Chen, K. H. *Chem. Mater.* **2004**, *16*, 2457. Chen, R. S.; Chang, H. M.; Huang, Y. S.; Tsai, D. S.; Chattopadhyay, S.; Chen, K. H. *J. Cryst. Growth* **2004**, *271*, 105. Chen, R. S.; Chang, H. M.; Huang, Y. S.; Tsai, D. S.; Chiu, K. C. *Nanotechnology* **2005**, *16*, 93. Korotcov, A. V.; Huang, Y. S.; Tsai, D. S.; Tiong, K. K. *Thin Solid Films* **2006**, *503*, 96. Korotcov, A.; Huang, Y. S.; Tsai, D. S.; Tiong, K. K. *J. Phys.: Condens. Matter* **2006**, *18*, 1121. Chen, R. S.; Korotcov, A.; Huang, Y. S.; Tsai, D. S. *Nanotechnology* **2006**, *17*, R67.

high vacuum chamber of 5×10^{-6} mbar for 1.5 h. The reduced sample was denoted as Ir−IrO_2NT if both Ir and IrO_2 reflections appeared in its X-ray diffraction (XRD) pattern. The sample was denoted as IrNT if only Ir metal reflections were detected. The Pt−Ir−IrO_2NT electrode was prepared by square-wave current pulse electrodeposition of Pt on Ir−IrO_2NT in 5 mM H_2PtCl_6 solution using a peak current density of 2.5 or 1.25 mA cm^{-2}. One duty cycle consisted of 3 s of on time and 3 s of off time. The total deposition times were 240 s for 2.5 mA cm^{-2} and 480 s for 1.25 mA cm^{-2}. The CVD deposited IrO_2 mass was 0.409 mg cm^{-2}, and the electrodeposited Pt mass was 0.100 mg cm^{-2}.

Morphology of nanotubes was examined using a field emission scanning electron microscope (FESEM, JEOL JSM6500F). Structural details Ir−IrO_2NT, Pt−IrO_2NT, and Pt−Ir−IrO_2NT were revealed by a high-resolution transmission electron microscope (HRTEM, FEI Tecnai F20 G2) operated at 200 kV. XRD patterns were recorded using a diffractometer equipped with a Cu Kα radiation source (Rigaku, D/Max-RC) at two scan rates, 10° min^{-1} in 20−100° and 0.5° min^{-1} in 38−44°. On the basis of the Scherrer formula, the Ir metal grain sizes were calculated using the broadened Ir(111) reflections in the slow-scan patterns. The Scherrer formula was written as $L = 0.9\lambda/(B \cos \theta)$, in which L is the crystal size, λ is the wavelength, and B is the full width at half-maximum at the Bragg angle θ. Surface compositions of the tubes were analyzed by X-ray photoelectron spectroscopy (XPS) using a Thermo VG Scientific Theta Probe system. The X-ray source was the Al Kα 1486.68 eV line, and the Ag $3d_{5/2}$ line at 368.26 eV was the calibration reference. XPS peak positions and integrated intensities were obtained through curve fitting using Avantage v2.13 Software.[12]

Working electrodes were prepared by mounting one of IrO_2NT, Ir−IrO_2NT, Pt−IrO_2NT, Pt−IrNT, and Pt−Ir−IrO_2NT on a copper plate and connecting the two with a conducting silver paint. All of the conducting surface of the working electrode was insulated with Miccrostop lacquer (Pyramid Plastics, Inc., Tolber Division) except the nanotubes, which were completely immersed in the electrolyte. For comparison, a PtRu working electrode was also prepared by dispersing the Johnson−Matthey PtRu (1:1) catalyst (HiSPEC 6000) in 5 wt % Nafion solution (274704, Aldrich) with a mass ratio of 2:1 and then coating the solution on a conducting graphite plate. The PtRu−graphite electrode was electrically insulated with Miccrostop except for an area of 1 cm^2 which was loaded with 0.6 mg of PtRu. The electrochemical measurements were performed using a three-electrode cell at 25 ± 1 °C. Potentials were measured against and are quoted versus a saturated Ag/AgCl electrode (XR820, Radiometer Analytical), if not specified otherwise. Electrolytes of 0.5 M H_2SO_4 were prepared using sulfuric acid (>99.9%) and ultrapure water (resistivity > 18 MΩ·cm, ROpure ST, Barnstead). The electrolyte was degassed by bubbling N_2 for 15 min before executing cyclic voltammetry (CV) measurement for CH_3OH and CO oxidation (Solartron 1287 potentiostat). The CO adsorption was carried out by bubbling CO through a previously deaerated electrolyte while holding the working electrode at 0.1 V (vs NHE).

Results and Discussion

Structure Characterization of IrO_2NT, Ir−IrO_2NT, and Pt−Ir−IrO_2NT. To synthesize PtIr electrocatalysts starting from IrO_2NT, subtracting the lattice oxygen of IrO_2 is necessary. Top and cross-sectional views of the nanotubes being reduced in the 500 °C annealing are illustrated in Figure 1. The vertically aligned square tubes are of height 1100 nm and diameter 80−100 nm. FESEM images of these tubes before reduction and being reduced at higher temperatures are not shown since their secondary electron images are no different from Figure 1a,b. Those subtle structural changes due to oxygen removal are mainly revealed in the TEM analysis.

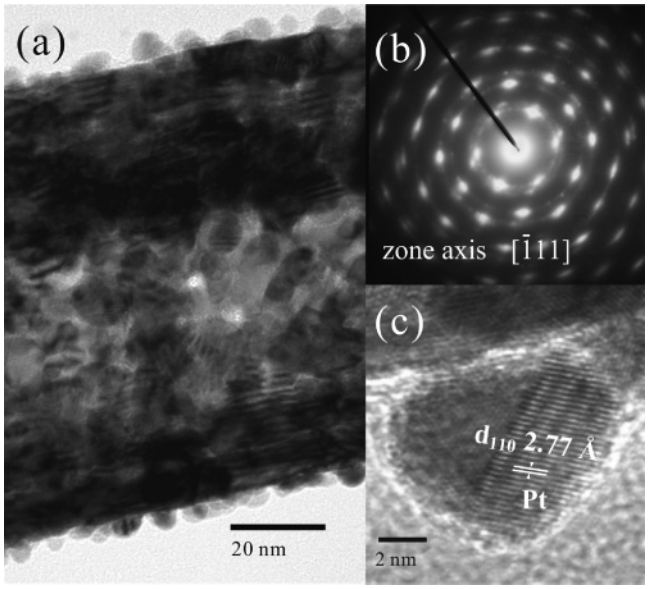

Figure 4. Structure of a Pt−Ir−IrO_2NT tube which was first 500 °C-reduced and then electrodeposited on Pt. (a) A bright-field TEM image on a section of the Pt−Ir−IrO_2NT tube, (b) an electron diffraction pattern, and (c) a HRTEM image of a 7 nm Pt particle deposited on the lower side of the tube wall.

The wall thickness of IrO_2NT is around 15 nm and thinner at the top, 8 nm. When the lattice oxygen is removed, the wall thickness decreases by 1 nm approximately, and the wall texture is fragmented. Variation in the wall texture is depicted in Figure 2a,b, which shows two bright-field TEM images of the upper section of an 85 nm diameter tube. Figure 2b indicates that the smooth wall of Figure 2a turns into a vermicular structure after 500 °C annealing while dimensions of the hollow square tube remain virtually unchanged. Since four Ir atoms of an Ir face-centered cubic (fcc) cell occupy 56.6 $Å^3$ in volume, while those of IrO_2 rutile crystal occupy 127.7 $Å^3$, a thin porous wall of 56% porosity is generated when the lattice oxygen is taken away. The HRTEM image of Figure 2c illustrates that the vermicular structure is composed of many connected tiny Ir grains with slit-shaped pores in between. The typical Ir grains are 3−5 nm in size, and one porous plate of the tubular wall is stacked with two to three layers of Ir grains. Furthermore, the lattice of Ir metallic grains is intimately associated with its parent IrO_2 rutile crystal. Each IrO_2 tube is grown in the [001] direction of rutile crystal. The plain wall of the square tube belongs to one of the four IrO_2{110} facets, as described in the previous publication.[11] The crystal structure of the dense IrO_2 plate seems to be capable of constraining the Ir nuclei so that the Ir fcc crystals are commonly oriented with the Ir[1$\bar{1}$0] direction parallel to the IrO_2 tube growth direction, as marked in Figure 2c. Clear atomic images of the Ir[$\bar{1}$11] zone axis are found at the central region of these

(12) *Avantage Software;* Thermo VG Scientific: West Sussex, U.K., 1979

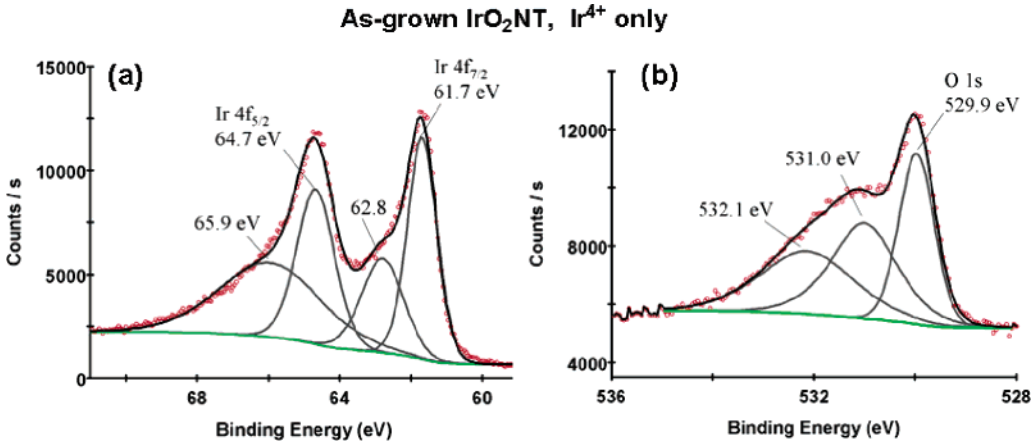

Figure 5. Peak fitted slow scan XPS spectra of (a) the Ir 4f {32.69 atom %} and (b) O 1s {67.31 atom %} lines of as-grown IrO_2NT.

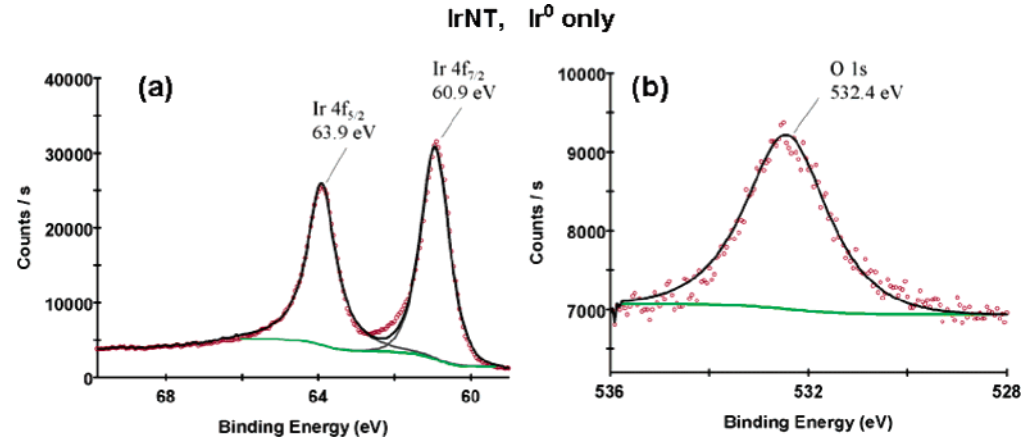

Figure 6. Peak fitted slow scan XPS spectra of (a) the Ir 4f {69.58 atom %} and (b) O 1s {30.42 atom %} lines of IrNT that had been reduced at 600 °C. The O 1s signal results from the surface oxygen, not the lattice oxygen.

Ir grains; meanwhile, lattice fringes corresponding to the Ir-{110} spacing can be observed near the Ir grain boundaries. Although not all Ir grains are strictly oriented in the same direction, this preferential orientation is obeyed by most of Ir grains, such as the grains marked as A−F in Figure 2c. It is also usual to observe that the lattice fringes of a underlying grain, such as the one that is located underneath the void among the C−E grains, comply with the preferential orientation imposed by IrO_2. Thus the preferential orientation is not a local but a widespread event in Ir nuclei. Also, we occasionally find a grain like G, which exhibits the {110} lattice fringes, but its lattice is disoriented at an angle with respect to the IrO_2 tube growth direction.

The XRD pattern of IrO_2NT consists of an IrO_2(002) reflection and a (300) reflection of the α-Al_2O_3 substrate because IrO_2 tubular crystals are grown in the [001] direction, as shown in the upper inset of Figure 3. When the oxygen removal begins, several Ir reflections emerge while the IrO_2 reflection fades out. As the annealing temperature increases, the Ir(111) reflection sharpens and the IrO_2(002) intensity decreases drastically. Figure 3 correlates a linear relation between the average Ir crystallite size and the annealing temperature and also presents the broadened (111) reflections being used in the size calculation. The average Ir crystal size at 500 °C is 4.5 nm, which is in line with the TEM observation. The Ir crystal size grows to 11.3 nm at 600 °C; meanwhile, the IrO_2 reflections vanish completely. The preferential orientation of Ir nuclei observed in TEM also influences the intensity ratio of Ir reflections. The intensity ratio of reflection (111) over (200) in the 600 °C pattern is 3.41, which is higher than that of randomly oriented Ir crystals 2.23.[13]

Figure 4a is a bright-field image of the upper section of a Pt−Ir−IrO_2 tube which was first reduced at 500 °C and then electrodeposited on Pt using a current density of 2.5 mA cm^{-2}. The pulse electrodeposited Pt particles are 2−8 nm in size, grown on an Ir−IrO_2 tube of 95 nm in diameter. Some of Pt particles block the pores generated during oxygen removal so that the number of pores appears less than that in Figure 2. Figure 4b, a typical electron diffraction pattern of the [$\bar{1}$11] zone axis on the tubular body, reveals an interesting crystallographic relation between Ir and Pt crystals. The unit cell parameter of the Pt fcc crystal is 3.92 Å,[14] slightly larger than that of Ir 3.84 Å.[13] Hence, the larger one of the two closely spaced rings belongs to Ir, and the inner ring belongs to Pt in the reciprocal space. If the Pt and Ir crystals are randomly oriented, two homogeneous rings ought to be presented. Nevertheless, Figure 4b is a pattern of weak rings with two sets of high-intensity spots of the [$\bar{1}$11] zone. These neighboring Pt and Ir fundamental spots suggest that the preferential orientation of Ir grains was partially transferred to the deposited Pt

(13) JCPDS card no. 87-0715. International Centre for Diffraction Data: Newtown Square, PA, 1997.
(14) JCPDS card no. 87-0646. International Centre for Diffraction Data: Newtown Square, PA, 1997.

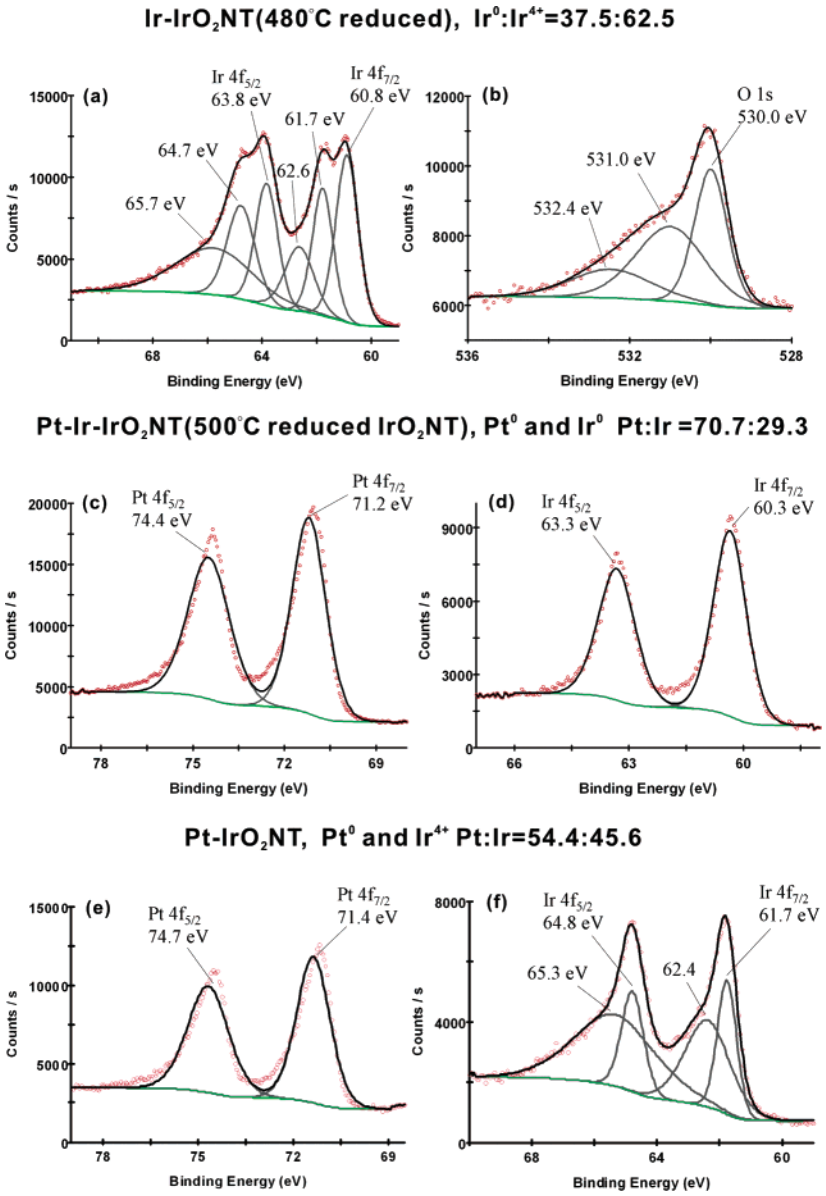

Figure 7. Peak fitted slow scan XPS spectra of (a) the Ir 4f {48.3 atom %} and (b) O 1s {51.7 atom %} lines of Ir−IrO_2NT that had been reduced at 480 °C. Part of the lattice oxygen survived the thermal annealing. The Ir^0/Ir^{4+} atomic ratio of the 480 °C-reduced surface is estimated to be 37.5:62.5. Slow scan XPS spectra of (c) the Pt 4f {70.7 atom %} and (b) Ir 4f {29.3 atom %} lines of Pt−Ir−IrO_2NT that had been reduced at 500 °C. No Ir^{4+} signal is found on the surface of Pt−Ir−IrO_2NT. Slow scan XPS spectra of (e) the Pt 4f {54.4 atom %} and (f) Ir 4f {45.6 atom %} lines of Pt−IrO_2NT. No Ir^0 is found, only the Ir^{4+} signal on the surface of Pt−IrO_2NT is found.

particles. A plausible explanation is that some of the Pt particles were grown epitaxially on the Ir grains. However, it was difficult to verify this epitaxial relation when focusing the tube body. The Pt and Ir lattices usually overlapped to form various moiré patterns in the phase contrast mode. The HRTEM image of a Pt particle in Figure 4c was recorded when focusing on one side of the tube. The fringe spacing on the right half of the Pt particle is about 0.227 nm, which corresponds to the (111) *d*-spacing of Pt fcc crystal. The less clear lattice fringe on its left half corresponds to the (110) *d*-spacing.

XPS Analysis of IrO_2NT, Ir−IrO_2NT, and Pt−Ir−IrO_2NT. XPS analysis provides essential surface information on the oxidation state and the stoichiometry of IrO_2NT, Ir−IrO_2NT, and Pt−Ir−IrO_2NT. Slow scans on the Ir 4f doublet (7/2 and 5/2) and oxygen O 1s peaks of IrO_2NT were carried out in the binding energy range of 56−72 eV and 526−540 eV, as illustrated in Figure 5. The Gaussian and Lorentzian mixing line shape was employed after the background treatment by the Shirley function in fitting to ensure accurate peak positions. Two binding states of Ir are identified as $4f_{7/2}$ and $4f_{5/2}$ at 61.7 and 64.7 eV, very close to those of the IrO_2 single crystal.[15] They are attributed to the 4+ oxidation state of Ir. Deconvolution of the Ir 4f scan reveals two extra broad features at 62.8 and 65.9 eV in the $4f_{7/2}$ and $4f_{5/2}$ regions. The O 1s signal appears to be a triplet, whose major peak at 529.9 eV is close to that of the IrO_2 single crystal at 529.7 eV.[15] The other two oxygen broad peaks are at 531.0 and 532.1 eV. The stoichiometry analysis shows excess oxygen of 1.9%, which indicates the presence of higher oxides on the IrO_2NT surface. More excess oxygen on the surface was

(15) Wertheim, G. K.; Guggenheim, H. J. *Phys. Rev. B* **1980**, *22*, 4680.

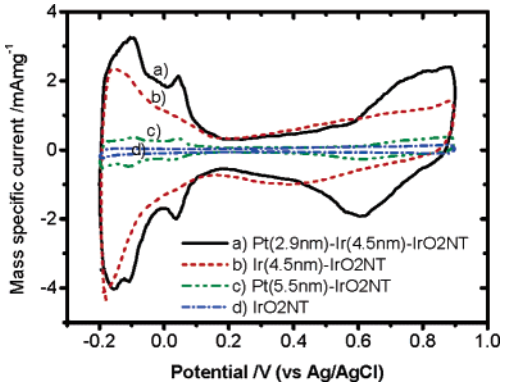

Figure 8. Cyclic voltammograms of (a) Pt(2.9 nm)−Ir(4.5 nm)−IrO_2NT, (b) Ir(4.5 nm)−IrO_2NT, (c) Pt(5.5 nm)−IrO_2NT, and (d) IrO_2NT, recorded in 0.5 M H_2SO_4 at 25 °C and 10 mV s^{-1}. Please note the evident hydrogen adsorption and desorption features in the two Pt-containing electrodes.

Table 1. Values of Mass Specific Surface Area of Various Electrodes Based on the Hydrogen Desorption and CO Stripping Voltammograms Measured in 0.5 M H_2SO_4 at 25 °C and 10 mV s^{-1} [a]

electrode	surface area[b] (H^+), m^2 g^{-1}	surface area[b] (CO), m^2 g^{-1}
Pt(2.9 nm)−Ir(4.5 nm)−IrO_2NT[c]	26.6	11.4
Pt(3.2 nm)−Ir(4.5 nm)−IrO_2NT[c]	16.6	8.68
Pt(5.1 nm)−Ir(11.3 nm)NT[d]	22.1	8.04
Pt(5.5 nm)−IrO_2NT	3.1	1.86
Ir(4.5 nm)−IrO_2NT[e]	16.9	16.4
Ir(11.3 nm)NT[e]	19.4	23.5
IrO_2NT[e]	1.6	N.A.

[a] The numbers in the electrode parentheses denote its Pt and Ir grain sizes. [b] All the mass specific values were based on the sum of the Pt plus the Ir masses, regardless of Ir existing in the metal or oxide form. [c] Pt(2.9 nm)−Ir(4.5 nm)−IrO_2NT and Pt(3.2 nm)−Ir(4.5 nm)−IrO_2NT electrodes were prepared by electrodepositing Pt on a 500 °C-reduced IrO_2NT, using galvanic square-wave currents of 1.25 and 2.5 mA cm^{-2}, respectively. [d] The Pt(5.1 nm)−Ir(11.3 nm)NT electrode was prepared by electrodepositing Pt on the 600 °C-reduced tubes, using a galvanic square-wave current of 2.5 mA cm^{-2}. [e] Ir(4.5 nm)−IrO_2NT and Ir(11.3 nm)NT were prepared by reducing IrO_2NT at 500 and 600 °C, respectively. IrO_2NT did not adsorb CO; there was no CO stripping peak.

reported on IrO_2 nanorods grown via MOCVD.[16]

Figure 6 shows the Ir 4f and O 1s core level electron peaks of 600 °C-reduced tubes, whose XRD pattern exhibited merely Ir metal and no IrO_2 reflections. The two Ir binding states of $4f_{7/2}$ and $4f_{5/2}$ are at 60.9 and 63.9 eV, which are typical values of Ir metal.[17] In contrast to the asymmetric Ir^{4+} 4f peak shape of IrO_2, the peak shape of the Ir^0 4f electron is nearly symmetric and properly described by the Gaussian and Lorentzian function. The O 1s signal of Figure 6b is at 532.4 eV, identified as the oxygen signal of the surface hydroxides, not the lattice oxygen. When the annealing temperature was set between 480 and 560 °C, the resultant XPS spectra bear the characteristics of both Figure 5 and Figure 6. A typical example is the XPS spectra of 480 °C-reduced sample, illustrated in Figure 7a,b. The Ir 4f scan in Figure 7a is deconvoluted into three pairs of peaks. The pair of $4f_{7/2}$ and $4f_{5/2}$ at 60.8 and 63.8 eV is attributed to Ir^0. The other two pairs at 61.7 and 64.7 eV and 62.6 and

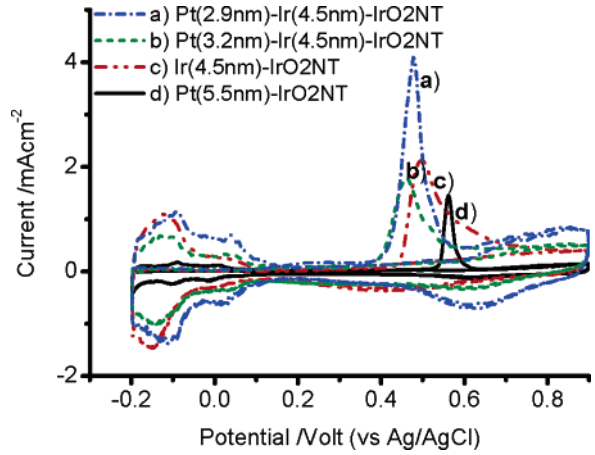

Figure 9. CO_{ad} stripping voltammograms of (a) Pt(2.9 nm)−Ir(4.5 nm)−IrO_2NT, (b) Pt(3.2 nm)−Ir(4.5 nm)−IrO_2NT, (c) Ir(4.5 nm)−IrO_2NT, and (d) Pt(5.5 nm)−IrO_2NT, measured in a 0.5 M H_2SO_4 carbon monoxide saturated solution at 25 °C and 10 mV s^{-1}. The CO adsorption was carried out at 0.1 V (vs NHE).

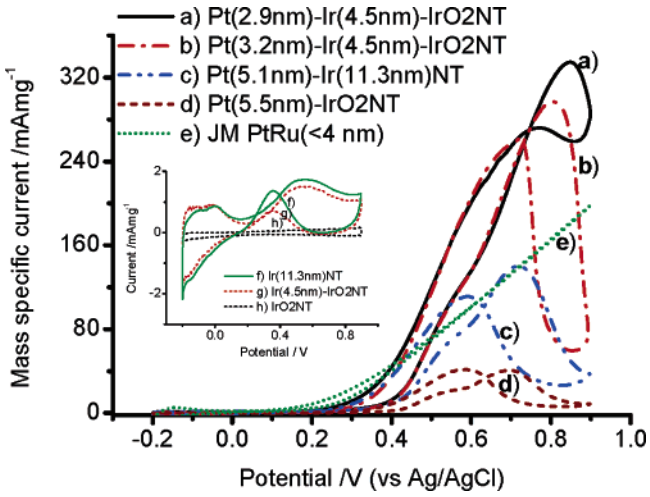

Figure 10. Cyclic voltammograms of (a) Pt(2.9 nm)−Ir(4.5 nm)−IrO_2-NT, (b) Pt(3.2 nm)−Ir(4.5 nm)−IrO_2NT, (c) Pt(5.1 nm)−Ir(11.3 nm)NT, (d) Pt(5.5 nm)−IrO_2NT, (e) HiSPEC 6000 Pt/Ru = 1:1 (Johnson−Matthey), (f) Ir(11.3 nm)NT, (g) Ir(4.5 nm)−IrO_2NT, and (h) IrO_2NT, measured in a solution containing 2.5 M methanol and 0.5 M H_2SO_4 at 25 °C and 10 mV s^{-1}.

65.7 eV are attributed to Ir^{+4}. The atomic ratio of coexisting Ir^0 and Ir^{4+} is estimated to be 37.5:62.5, according to the deconvoluted peak areas. Also shown in Figure 7c,d are the Pt 4f and Ir 4f scans of Pt−Ir−IrO_2NT, which is the most active electrode in this work. Even though Pt−Ir−IrO_2NT of Figure 7 was reduced at 500 °C and shows IrO_2 XRD reflections, its surface contains only Pt^0 and Ir^0; no Ir^{4+} is found. In comparison, the Pt 4f and Ir 4f scans of Pt−IrO_2-NT are plotted in Figure 7e,f. The Ir 4f scan in Figure 7f is nearly identical with that in Figure 5a of IrO_2NT. The peak positions of Pt 4f scan (71.4, 74.7 eV) in Figure 7e are slightly higher than those of the Pt 4f scan (71.2, 74.4 eV) of Pt−Ir−IrO_2NT. Judging from a high Ir^0 surface fraction in Figures 6 and 7, we conclude that the oxygen removal initiates from the tube surface of IrO_2NT. Regarding catalyst preparation, 500 °C seems to be an optimal thermal annealing temperature since an entire Ir metal surface was created before the tiny Ir crystallites grew large.

(16) Chen, R. S.; Huang, Y. S.; Liang, Y. M.; Tsai, D. S.; Chi, Y.; Kai, J. J. *J. Mater. Chem.* **2003**, *13*, 2525.
(17) Moulder, J. F.; Stickle, W. F.; Sobol, P. E.; Bomben, K. D. *Handbook of X-ray Photoelectron Spectroscopy*; Physical Electronics, Inc.: Eden Prairie, MN, 1995; pp 178−179 and 180−181.

Table 2. Peak Current Densities (i_P) and Peak Potentials (E_P) of the IrO_2NT-Derived Catalysts and the Johnson−Matthey HiSPEC6000 PtRu(1:1) Catalyst in CV, Which Was Performed in a Solution of 2.5 M Methanol (MeOH) and 0.5 M H_2SO_4 at 25 °C and 10 mV s^{-1}

	MeOH (positive)		MeOH (negative)		CO_{ad} stripping
electrode	i_P (mA mg^{-1})[a]	E_P (V)	i_P (mA mg^{-1})[a]	E_P (V)	E_P (V)
Pt(2.9 nm)−Ir(4.5 nm)−IrO_2NT	336	0.85	273	0.75	0.47
Pt(3.2 nm)−Ir(4.5 nm)−IrO_2NT	298	0.80	262	0.72	0.50
Pt(5.1 nm)−Ir(11.3 nm)NT	141	0.72	111	0.59	0.47
Pt(5.5 nm)−IrO_2NT	41.6	0.71	43.9	0.66	0.56
JM PtRu(1:1)	196	0.90	196	0.90	0.32

[a] Values of the mass specific current densities were based on the sum of Pt plus Ir mass, regardless Ir existed in form of metal or oxide.

Catalytic Activities in CO and Methanol Oxidation. One of the motivations in removing the lattice oxygen of IrO_2NT is to raise the surface area of the derived catalyst near those of state-of-the-art catalysts. Figure 8 compares two types of CV diagrams in 0.5 M H_2SO_4. One type belongs to those electrodes that had undergone 500 °C thermal annealing, and the other type belongs to those that had not. The electrodes of Pt(2.9 nm)−Ir(4.5 nm)−IrO_2NT and Ir(4.5 nm)−IrO_2NT exhibit much higher response current densities than the electrodes of Pt(5.5 nm)−IrO_2NT and IrO_2NT, because of fragmentation and Ir nucleation on the tube wall. The number in parentheses immediately following Pt or Ir indicates its grain size. Integrating the hydrogen desorption charge between −0.2 and 0.2 V and subtracting the double-layer charge from the CV diagrams yielded the values of the electrochemical active surface area in Table 1. A hydrogen charge density of 210 μC cm^{-2} was assumed for the Pt surface,[18] and that of 220 μC cm^{-2} was assumed for the Ir surface.[19] Surface area values of Ir−IrO_2NT and its derived electrodes are apparently higher. Specifically, comparing two electrodes of the same Pt loading, the Pt(2.9 nm)−Ir(4.5 nm)−IrO_2NT surface area of 26.6 m^2 g^{-1} is much larger than that of Pt(5.5 nm)−IrO_2NT, 3.1 m^2 g^{-1}. Additionally, it is worth noting a strong resemblance between the Ir(4.5 nm)−IrO_2NT CV (curve b in Figure 8) and the Ir(110) CV reported by Gomez and Weaver.[19] The Ir(4.5 nm)−IrO_2NT CV is featured with a pair of peaks for hydrogen adsorption (−0.18 V) and desorption (−0.15 V) in the low potential region and the other two very broad peaks for hydroxide adsorption (0.67 V) and desorption (0.38 V) in the high potential region. Almost the same feature was reported on the Ir(110) single crystal in 0.1 M $HClO_4$. We also reproduced the above characteristics of Ir(4.5 nm)−IrO_2NT in 0.1 M $HClO_4$.

Also listed in Table 1 are the surface areas calculated from the integrated peak area of the CO stripping voltammogram, correcting for the double-layer charge and assuming a Coulombic charge of 420 μC cm^{-2} for the linearly adsorbed CO.[20] The CO_{ad} stripping voltammograms of Pt(2.9 nm)−Ir(4.5 nm)−IrO_2NT, Pt(3.2 nm)−Ir(4.5 nm)−IrO_2NT, Ir(4.5 nm)−IrO_2NT, and Pt(5.5 nm)−IrO_2NT are presented in Figure 9. The peak potential of Pt(5.5 nm)−IrO_2NT is the highest among the four electrodes, 0.56 V, which is slightly lower than that of Pt nanoparticles reported in the literature.[20] On the other hand, the reduced nanotubes, with or without Pt, are quite capable of adsorbing and oxidizing CO. The onset and the peak potentials of Ir(4.5 nm)−IrO_2NT are 0.41 and 0.50 V, respectively. The CO oxidation peak of Ir(4.5 nm)−IrO_2NT displays a long tail, extending to 0.80 V. The peak shape of Ir(4.5 nm)−IrO_2NT is quite similar to that of Ir(110), reported by Gomez and Weaver in 0.1 M $HClO_4$ at 23 °C and 50 mV s^{-1}; except the peak potential of 0.4 V (vs SCE) is lower, and the peak tail extends to 0.65 V (vs SCE).[21]

Figure 10 displays the catalytic activities of four IrO_2NT−derived electrodes in the methanol oxidation reaction. The CV diagrams of the electrodes without Pt are plotted in the inset. The activity of IrO_2NT in methanol oxidation is negligible. The reduced form of IrO_2NT exhibits some catalytic activity, with the activity of Ir(11.3 nm)NT somewhat higher than that of Ir(4.5 nm)−IrO_2NT. The methanol oxidation activity soars after depositing 0.1 mg cm^{-2} Pt on Ir(4.5 nm)−IrO_2NT, judging from 2 orders of magnitude gain in response current. The Pt catalysis in methanol oxidation strongly depends on the underlying Ir. The current densities of three PtIr electrodes are considerably higher than that of Pt(5.5 nm)−IrO_2NT. Furthermore, the activity of the PtIr electrode strongly depends on its Ir grain size. The current at 0.72 V in the forward sweep is 249 mA mg^{-1} for Pt(3.2 nm)−Ir(4.5 nm)−IrO_2NT, 79% higher than 140 mA mg^{-1} for Pt(5.1 nm)−Ir(11.3 nm)NT. The Pt particle size is also a factor. The response current of Pt(2.9 nm)−Ir(4.5 nm)−IrO_2NT is nearly identical with that of Pt(3.2 nm)−Ir(4.5 nm)−IrO_2NT at a potential < 0.7 V. The response current of Pt(2.9 nm)−Ir(4.5 nm)−IrO_2NT is higher than that of Pt(3.2 nm)−Ir(4.5 nm)−IrO_2NT in the potential range of 0.7−0.9 V. For comparison, we also plot the response current of Johnson−Matthey PtRu (1:1) catalyst in Figure 10. The response current of PtRu is higher than that of Pt(2.9 or 3.2 nm)−Ir(4.5 nm)−IrO_2NT in the low potential range (<0.4 V) but lower in the high potential range (>0.4 V). The PtRu peak potential of 0.32 V in CO stripping in Table 2 suggests that the less ideal performance of PtIr in the low potential (<0.4 V) is related to its CO oxidation potential. Values of the peak response currents and potentials of methanol oxidation in the forward and backward sweeps of Figure 10 are listed in Table 2. Also listed are the peak potentials of CO_{ad} stripping.

(18) Tran, T. D.; Langer, S. H. *Anal. Chem.* **1993**, *65*, 1805.
(19) Gomez, R.; Weaver, M. J. *Langmuir* **2002**, *18*, 4426.
(20) Kawaguchi, T.; Sugimoto, W.; Murakami, Y.; Takasu, Y. *Electrochem. Commun.* **2004**, *6*, 480.
(21) Gomez, R.; Weaver, M. J. *Langmuir* **1998**, *14*, 2525.

Conclusion

A PtIr structural electrocatalyst has been derived from IrO_2-NT which is an assembly of vertical aligned thin-wall tubes grown in CVD. The lattice oxygen removal from IrO_2NT is identified as a critical step in achieving the catalyst activity. The Ir metallic grains that nucleate in lattice oxygen removal are preferentially oriented with its [110] direction parallel to the growth direction of IrO_2[001]. The HRTEM images of different Ir grains are featured with the same lattice fringe of {110} spacing. The CV diagram of reduced nanotubes displays the characteristics of the Ir(110) plane. Fragmentation in the tubular wall of IrO_2NT increases the surface area significantly. A proper amount of Pt electrodeposition on the reduced nanotubes yields a catalyst with activity comparable to that of the commercial PtRu catalyst.

Acknowledgment. The authors acknowledge the financial support of National Science Council of Taiwan under the Project Nos. NSC95-2120-M-011-001 and NSC94-2120-M-011-001.

CM062085U